Journal of Power Sources 234 (2013) 1–7

Contents lists available at SciVerse ScienceDirect

Journal of Power Sources

journal homepage: www.elsevier.com/locate/jpowsour

Anomalous effect of K ions on electrochemical capacitance of amorphous MnO_2

Chunguang Wei [a,b], Chengjun Xu [a], Baohua Li [a], Hongda Du [a], Ding Nan [b], Feiyu Kang [a,b,*]

[a] City Key Laboratory of Thermal Management Engineering and Materials, Graduate School at Shenzhen, Tsinghua University, Shenzhen, Guangdong 518055, China
[b] State Key Laboratory of New Ceramics and Fine Processing, Department of Materials Science and Engineering, Tsinghua University, Beijing 100084, China

HIGHLIGHTS

- Describe a fundamental study which correlates the effect of added potassium on the electrochemical response of MnO_2.
- The effect of K ion content on the electrochemical capacitance properties of amorphous MnO_2 was investigated systematically.
- M2, M4 and M6 have bigger specific capacitance, surface area and more pores than M8, M10, and M12.
- Part of K ions in the MnO_2 tunnels can be replaced by Na ions during electrochemical reaction.

GRAPHICAL ABSTRACT

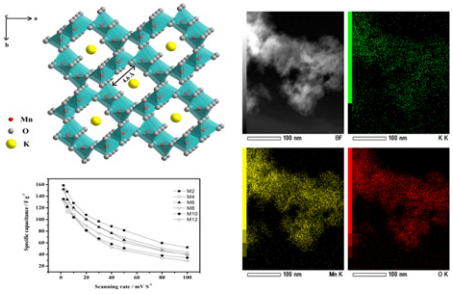

ARTICLE INFO

Article history:
Received 2 August 2012
Received in revised form
15 December 2012
Accepted 19 January 2013
Available online 29 January 2013

Keywords:
Manganese dioxide
Nanoparticle
K ion
pH
Amorphous
Specific capacitance

ABSTRACT

Six samples of α-MnO_2 with different K ion contents are synthesized by using $KMnO_4$ and $Mn(CH_3COO)_2{\cdot}4H_2O$ with different pH values at room temperature. The samples are labeled as M*x* where *x* denotes the pH value. The anomalous effect of K ion content on the electrochemical capacitance properties of amorphous MnO_2 is investigated systematically. It is found that with the increase of the K ion content, the MnO_2 nanospheres form a more dense aggregates, the surface area dramatically decreases from 273 (M2) to 14 $m^2\ g^{-1}$ (M12), and pore volume decreases from 0.349 (M2) to 0.014 $cm^3\ g^{-1}$ (M12). The specific capacitance (SC) is decreased by 17.6% from 157 (M2) to 131 F g^{-1} (M12). In addition, the SC values are greatly influenced by the molar ratio of K to Mn in the range of 0–0.4. And it is found that part of K ions in the MnO_2 tunnels can be replaced by Na ions during electrochemical reaction. Finally, an appropriate explanation of the effect of K ion content on the SC values is provided.

1. Introduction

Electrochemical capacitors (ECs) or supercapacitors (ESCs), which is a power-type energy storage device that can provide a very high power density and a long cycle-life, have been received enormous attention [1–4]. ECs usually are an auxiliary power sources ranging from mobile devices to electric vehicles. The capacitance comes from two aspects: electric double-layer capacitance (EDLC) and pseudo-capacitance [5,6].

Various active materials used in ECs can be divided into three categories: (i) carbon based materials [3,7] which is now widely used in commercial products [8], (ii) conducting polymers [9,10], and (iii) transition-metal oxides [11,12]. Since Lee and Goodenough [13] first reported its capacitive behavior in mild solutions, manganese dioxide (MnO_2), among the transition-metal oxides [14],

* Corresponding author. City Key Laboratory of Thermal Management Engineering and Materials, Graduate School at Shenzhen, Tsinghua University, Shenzhen, Guangdong 518055, China. Tel./fax: +86 755 2603 6188.
E-mail address: fykang@tsinghua.edu.cn (F. Kang).

0378-7753/$ – see front matter © 2013 Elsevier B.V. All rights reserved.
http://dx.doi.org/10.1016/j.jpowsour.2013.01.126

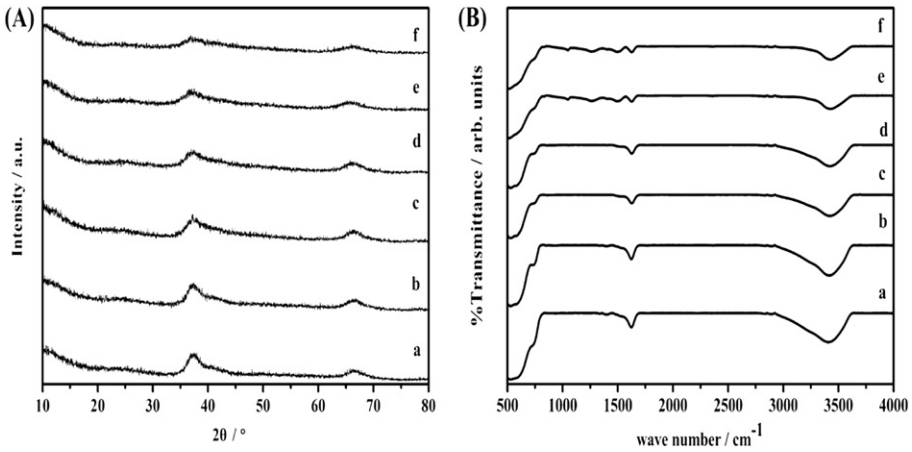

Fig. 1. (A) XRD patterns and (B) FTIR Spectrum of samples: (a) M2, (b) M4, (c) M6, (d) M8, (e) M10, and (f) M12.

has attracted attention for studies [4,15–21], because it is cheap, nontoxic, environmentally friendly and abundance in raw material.

The basic crystal structure of manganese dioxide configures of one manganese atom surrounded by six oxygen atoms to form an octahedron. Those MnO_6 octahedral subunits share vertices and edges to form crystalline tunnel structures [22,23]. Since capacitance properties are caused by the insertion and de-insertion of alkaline metal cations or protons into and from MnO_2 tunnel [24,25], it is believed that the nanoscale structure design and synthesis of MnO_2 is the key to improve its capacity. Dimensionality, morphology and particle size of MnO_2 have been regarded as critical factors to its exciting physicochemical properties [5,26].

It is believed that a small amount of cations, such as Li^+, Na^+, K^+, NH_4^+, or H_3O^+ is required to stabilize the tunnels [15] in the formation of MnO_2 by the oxidation of divalent manganese salt to obtain amorphous α-MnO_2. Based on the redox reactions of Mn^{4+} and Mn^{2+}, many methods have been developed to synthesize various crystallographic MnO_2. Since most of them use potassium permanganate ($KMnO_4$) as oxidant [20,27–29], most of MnO_2 contains K ions in the tunnel. However, studies on the effect of K ions on the performance of manganese dioxide capacitance remain rare.

In this paper, amorphous MnO_2 with different K ion contents are synthesized by using a common liquid co-precipitation method based on the redox reactions of Mn^{4+} and Mn^{2+} at room temperature. The content of K ions was controlled by changing the proportional amount of the solution of KOH and HCl. All samples are characterized by both physicochemical and electrochemical methods. The effect of K ion contents on the physical and electrochemical properties of amorphous MnO_2 has been systematically studied. Finally, an appropriate explanation for the effect of K ion content on the variations of SC values is provided.

2. Experimental section

All chemical reagents are analytical grade without further purification. And all aqueous solutions were prepared using deionized water.

2.1. Synthesis of α-MnO_2 samples

The MnO_2 powders were synthesized by redox reaction between Mn^{4+} and Mn^{2+} by chemical co-precipitation method. 1.58 g $KMnO_4$ and 3.68 g $Mn(CH_3COO)_2{\cdot}4H_2O$ were individually dissolved in 50 mL of de-ionized water by stirring continuously at room temperature for 30 min. The $Mn(CH_3COO)_2{\cdot}4H_2O$ solution was then added drop-wisely into the $KMnO_4$ solution under stirring

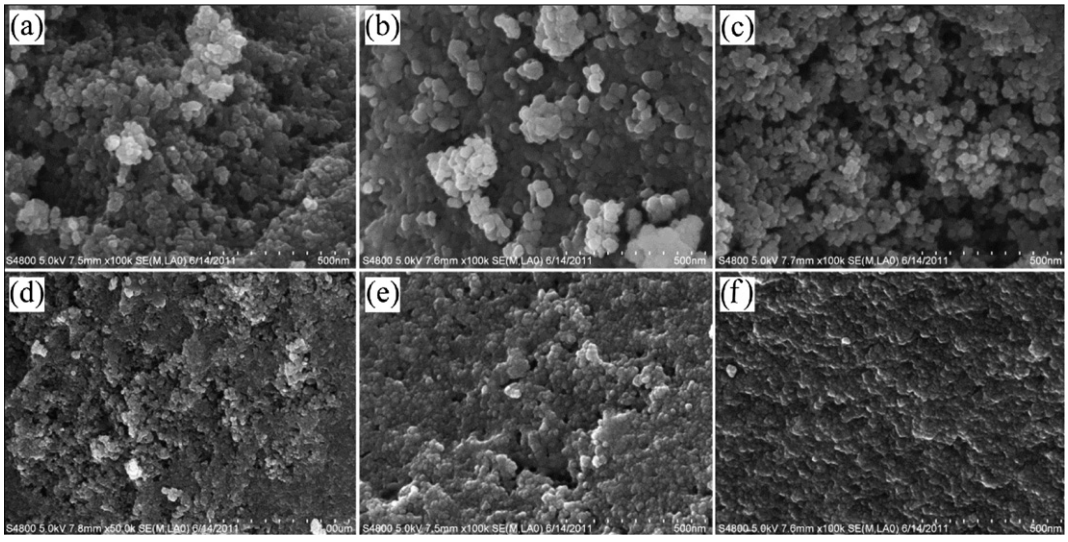

Fig. 2. SEM images of samples: (a) M2, (b) M4, (c) M6, (d) M8, (e) M10, and (f) M12.

continuously for 5 min to form a homogeneous solution whose pH value was controlled at 2, 4, 6, 8, 10, or 12 by using a solution of KOH and HCl. The resultant solution was stirred for 4 h at ambient temperature to form dark brown precipitates which were filtered and washed several times with deionized water, and finally dried at 85 °C in air for 12 h. The samples of α-MnO_2 with different K-ion contents were labeled as M*x*, where *x* stands for the pH value of the reaction solution, For example, M2, M4, M6, M8, M10, and M12 represent the samples for the pH values of reaction solutions at 2, 4, 6, 8, 10, and 12, respectively.

2.2. Characterization

Powders of the product samples were characterized by X-ray diffraction (XRD) using Rigaku 2500 powder diffractometer (Cu Kα radiation, $\lambda = 1.54056$ Å). The patterns were recorded over the 2θ angle of 10–80° at 40 kV, 30 mA, with a step size of 0.02°. The morphologies of the sample were observed by a field emission scanning electron microscopy (SEM) of HITACHI S4800, operated at beam energy of 10 kV. The low- and high-resolution images were obtained by a high resolution transmission electron JEOL-2011 microscope (HRTEM). XPS studies were conducted with a Physical Electronics PHI5802 instrument using X-rays magnesium anode (monochromatic Kα X-rays at 1253.6 eV) as a source. The C 1s region was used as a reference and was set at 284.8 eV. The Mn/K molar ration was analyzed by inductively coupled plasma-atomic emission spectroscopy (ICP-AES, ICPS6300). Fourier transform IR (FTIR) spectroscopy analysis was carried out by Nicolet Magana-IR 550/560 spectrophotometer, at the weight ratio of sample to KBr of 1:100.

The surface area and pore volume of the sample were determined by nitrogen gas adsorption at 77 K with an automated adsorption apparatus (Micrometrics, ASAP 2020). The surface area was determined from the Brunauer–Emmett–Teller (BET) equation. The total pore volume was calculated from a point on the isotherm at a relative pressure above 0.98. The pore size distribution was determined by BJH method from the desorption isotherm.

2.3. Electrochemical characterization

Electrodes were prepared by mixing 70 wt% of MnO_2 powder as active material with 20 wt% acetylene black and 10 wt% polytetrafluoroethylene (PTFE) as binder. 35 mg of MnO_2 powder and 10 mg of acetylene black were first mixed and dispersed in ethanol by ultrasonic stirring for 30 min. The solution was then dried at 80 °C for 12 h and 100 mg of PTFE aqueous solution (5 wt%) was added to form a paste. Then the paste was dried at 80 °C and a few drops of 1-methy-2-pyrrolidinone (NMP) were added to form syrup. The syrup was rolled into thick films. Finally, the films were cut into 1 cm × 1 cm pieces, each of about 2 mg weight, which were hot-pressed at 80 °C under 100 MPa pressure on a stainless steel mesh.

Electrochemical characterization, including cyclic voltammetry (CV) test, galvanostatical charge/discharge test and capability measurement, were carried out by using a VMP3 multichannel electrochemical station (Bio-Logic Corp, France). The electrochemical test by three-electrode method uses a platinum foil as counter electrode, a saturated calomel electrode (SCE) as reference electrode, and 0.1 M $NaSO_4$ as electrolyte. The CV measurements were carried out at scanning rates ranging from 2 to 100 mV s^{-1} and the potential range was from 0 to 1 V versus SCE in 0.1 M $NaSO_4$.

Table 1
Surface and pore characteristics as derived from nitrogen gas adsorption data.

Sample	S_{BET} ($m^2\ g^{-1}$)	S_{mic} ($m^2\ g^{-1}$)	S_{mes} ($m^2\ g^{-1}$)	S_{mes}/S_{BET} (%)	V ($cm^3\ g^{-1}$)	V_{micro} ($cm^3\ g^{-1}$)
M2	273.2	40.6	232.6	85.1%	0.349	0.016
M4	257.8	68.5	189.2	73.4%	0.341	0.029
M6	224.6	25.6	199	88.6%	0.389	0.009
M8	89.5	23.2	66.3	74.1%	0.064	0.010
M10	18.5	5.1	13.4	72.4%	0.023	0.002
M12	14.4	3.7	10.7	74.3%	0.014	0.002

3. Results and discussion

3.1. Characteristics

The XRD patterns of the product samples obtained from synthesis under different reaction-solution pH values at ambient temperature are shown in Fig. 1(A). Two broad peaks around $2\theta = 37.0°$ and 65.8° are clearly seen in Fig. 1(A), indicating the amorphous nature. These two peaks correspond to the same peaks of α-MnO_2 (JCPDS:No. 44-0141). The two broad peaks became weaker as the pH value increases from M2 to M12, which indicate that the sample became more amorphous under less acidic conditions.

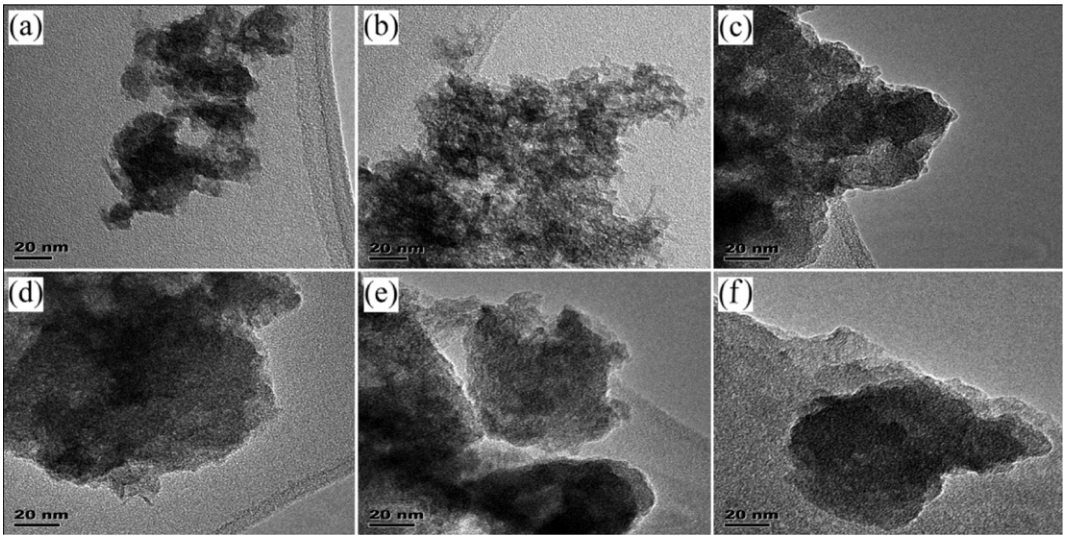

Fig. 3. TEM images of samples: (a) M2, (b) M4, (c) M6, (d) M8, (e) M10, and (f) M12.

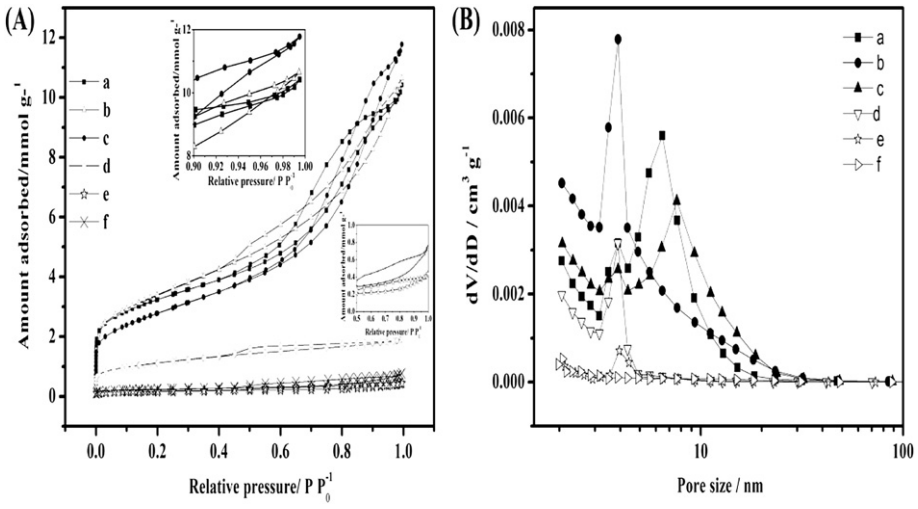

Fig. 4. (A) Nitrogen adsorption/desorption isotherms at 77 K and (B) pore size distribution calculated by BJH method for samples: (a) M2, (b) M4, (c) M6, (d) M8, (e) M10, and (f) M12.

Fig. 1(B) shows the FTIR spectra of the samples, where the peaks are observable at 3401, 1623, 1398, and 530 cm^{-1}. The broad band around 3401 cm^{-1} and the 1623 and 1402 cm^{-1} bands are normally attributed to stretching and bending vibrations of H–O–H, respectively [15]. The broad band around 500–700 cm^{-1} observed for all samples are ascribed to Mn–O bending vibration in MnO_6 octahedral [30,31]. The FTIR results indicate the presence of some bound water in the as-prepared sample.

The surface morphology of samples is shown in Fig. 2. It is seen that all the samples have similar ball-like morphology. The diameter of nano-spheres is about 20 nm. The diameter remains almost no change with different reaction conditions. Moreover Fig. 2e and f shows that the MnO_2 nano-spheres aggregate with one another to form more dense aggregates. The TEM images of the samples as shown in Fig. 3 reveal also clearly that the samples are amorphous.

The specific surface area was calculated by BET equation, surface and pore characteristics are summarized in Table 1. The S_{BET} value of samples decreases drastically with the increase of the solution pH value, from 273.2 $m^2\ g^{-1}$ (M2) to 14.4 $m^2\ g^{-1}$ (M12). Note that there are sudden drops of the results of S_{BET}, S_{mes}, and V from M6 to M8 samples. The total pore volumes of M2, M4, and M6 (acidic conditions) are much large than that of M8, M10, and M12 (basic conditions). These differences indicate that the samples M2, M4, and M6 are more porous than M8, M10, M12, as confirmed by the SEM images (Fig. 2).

The isotherms of nitrogen and adsorption/desorption of the samples are shown in Fig. 4(A). The isotherms show bigger difference between the acidic conditions (M2, M4, and M6) and basic conditions (M8, M10, and M12). Although all the isotherms of samples are typical of mesoporous materials with a hysteresis loop for relative pressure (P/P_0) ranging between 0.5 and 0.95, in correspondence to Type IV, the amount adsorbed as shown in Fig. 4(A), of the samples obtained from synthesis under basic conditions, is very small compared with the samples M2, M4, M6 (under acidic conditions).

Fig. 4(B) shows the pore size distribution of the six samples using the BJH method. It is clear that almost all the sample have a peak near 4 nm except the sample M12. Unlike M4, M6 have two broad peaks in the curve, M2, M8, M10 only has a dominant peak near 4 nm. Considering the surface morphology of M2, M4, and M6 which consists of nanospheres gathered together loosely, the porous structure caused the relatively high specific surface area.

In order to explore the property difference of the as-prepared samples, XPS has been used to character the element and the relative amount of the element. Fig. 5 exhibits the XPS spectra for

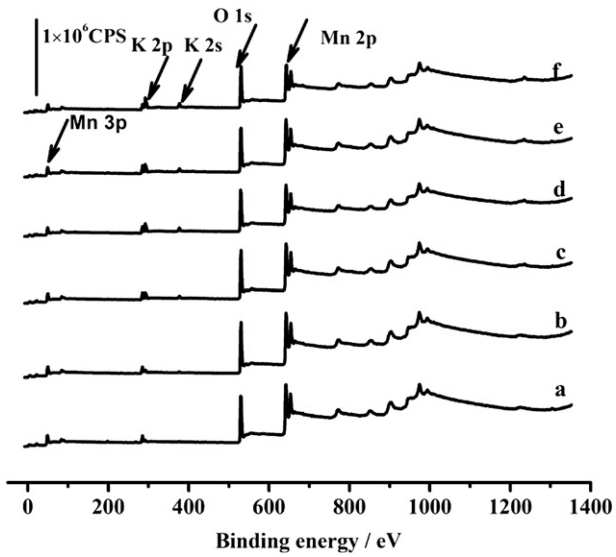

Fig. 5. XPS spectra of samples: (a) M2, (b) M4, (c) M6, (d) M8, (e) M10, and (f) M12.

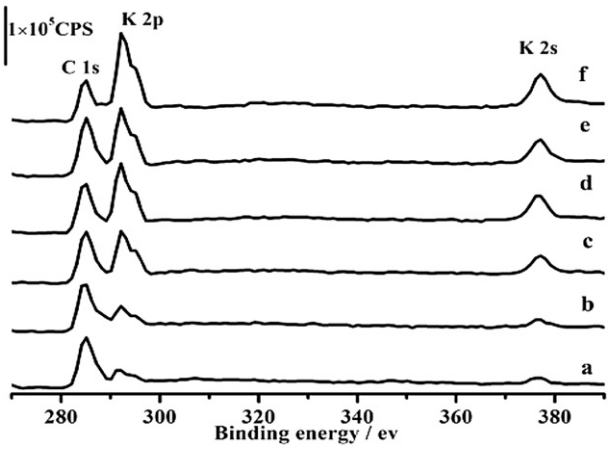

Fig. 6. Enlarged K 2s and K 2p XPS spectra of samples: (a) M2, (b) M4, (c) M6, (d) M8, (e) M10, and (f) M12.

Table 2
Contents of Mn, O, and K ions in the as-prepared samples.

At%	M2	M4	M6	M8	M10	M12
Mn	30.11	29.09	26.70	26.55	24.73	23.73
O	67.71	67.98	66.28	63.99	64.85	62.01
K	2.18	2.93	7.02	9.47	10.42	14.27
K/Mn	0.07	0.10	0.26	0.36	0.42	0.60

as-prepared samples. The Mn 2p, O 1s, K 2s and K 2p peaks are clearly seen in the figure to indicate the existence of K in all samples. Furthermore, as seen from the enlarged scale shown in Fig. 6, the intensity of K 2s and K 2p peaks increased gradually from M2 to M12, implying that the K^+ content increased from M2 to M12.

The K, Mn and O content of the as-prepared samples are presented in Table 2. The results of Mn and K were characterized by ICP elemental analyses, and the content of O was tested by XPS analyses. The result is in accord with the XPS survey spectra. The distribution of Mn, O and K element is shown in Fig. 7. It is seen that all three elements are very uniform and there is no obvious aggregation of any elements.

From the above characteristics, including XRD pattern, SEM, TEM, nitrogen adsorption, XPS and ICP elemental analyses, all the samples are α-MnO_2 and have the same tunnel structure, with little change in its surface morphology. The main difference among them is the content of K ions, which was speculated as the main reason for the samples showing great difference on surface morphology, BET surface, and pore structure. The tunnel size of the α-MnO_2 (2 × 2) is ∼4.6 Å, which is suitable for the insertion/extraction of alkali cations [32]. Brock et al. [33] reported that a small amount of cations such as Li^+, K^+, NH_4^+, Ba^{2+} or H_3O^+ is required to stabilize the tunnels in the formation of α-MnO_2.

3.2. Electrochemical properties

The specific capacitance (SC) of MnO_2 is mainly characterized by the crystal structure of MnO_2 [15]. Other physicochemical properties, such as surface area, porosity, surface area, and morphology, may also influence the SC values [15].

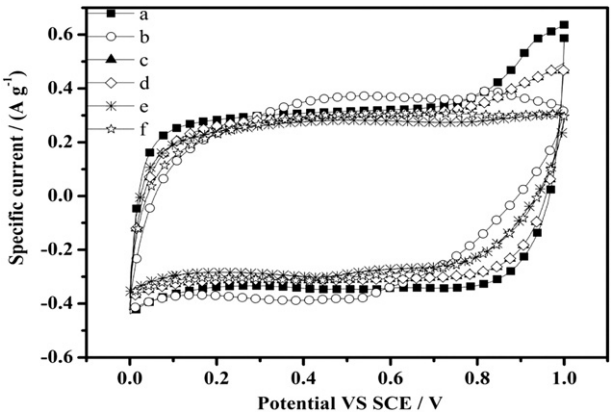

Fig. 8. Cyclic voltammograms of samples: (a) M2, (b) M4, (c) M6, (d) M8, (e) M10, and (f) M12, recorded between 0 and 1.0 V vs SCE in 0.1 M Na_2SO_4 aqueous solution at a sweep rate of 2 mV s^{-1}.

There are two mechanisms proposed to clarify the charge storage mechanism in MnO_2. The first mechanism is the tunnel storage mechanism (TSM), which involves intercalation/extraction of protons (H_3O^+) or alkali cations (M^+) from/into the electrolyte into/from the tunnel of MnO_2. This mechanism is presumed to be predominant in crystalline MnO_2 [34], as expressed by the following equation [15,24,25]:

$$MnO_2 + M^+ + e^- \rightarrow MnOOM\ (M^+ = Li^+, Na^+, K^+, \text{or } H_3O^+) \quad (1)$$

The second mechanism is the surface chemisorption mechanism (SCM), which based on the surface adsorption/desorption of cations from/into the electrolyte [35],:

$$(MnO_2)_{surface} + M^+ + e^- \rightarrow (MnOOM)_{surface}\ (M^+ = Li^+, Na^+, K^+, \text{or } H_3O^+) \quad (2)$$

This surface process is likely to be predominant in amorphous MnO_2 [34].

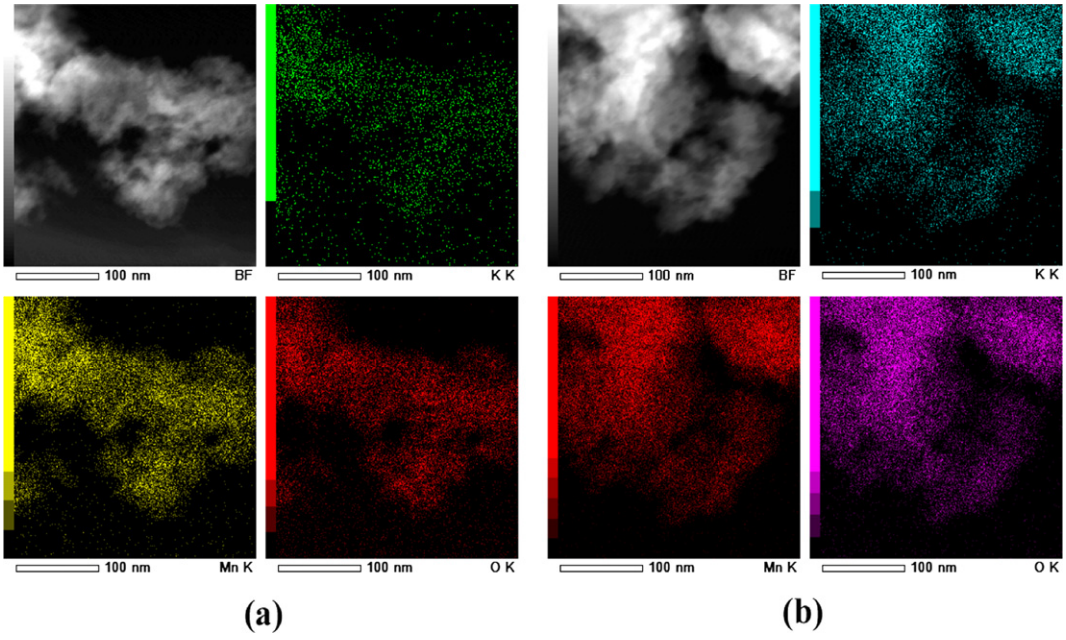

Fig. 7. TEM mapping images of K, Mn and O for samples: (a) M2 and (b) M12.

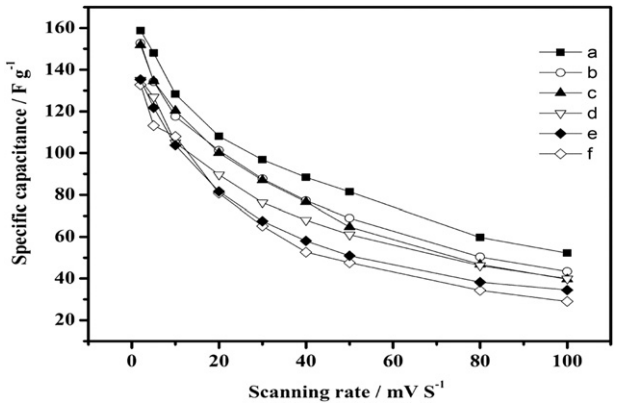

Fig. 9. Dependence of SC on scanning rate for samples: (a) M2, (b) M4, (c) M6, (d) M8, (e) M10, and (f) M12, recorded between 0 and 1.0 V vs SCE in aqueous 0.1 M Na_2SO_4 aqueous electrolyte.

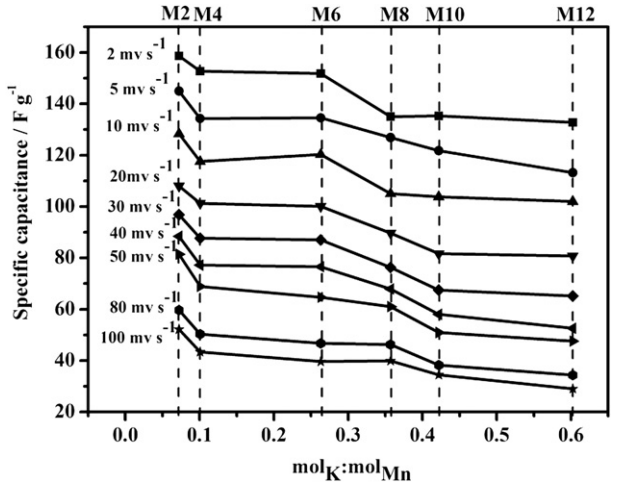

Fig. 10. Dependence of specific capacitance of as-prepared samples on molar ration of K to Mn.

The specific capacitance (SC) of the samples can be determined by obtaining firstly the charge (Q) as half of the integrated area of the CV curve, and subsequently dividing the charge by the mass of the active material (m) and the width of the potential window (ΔV):

$$C = \frac{Q}{\Delta V \times m} \tag{3}$$

Electrochemical measurements of the performance of electrodes, which are fabricated using different as-prepared samples, were conducted in 0.1 M Na_2SO_4 aqueous electrolyte. Fig. 8 shows the CV curves of the samples recorded between 0 and 1.0 V versus saturated calomel electrode (SCE) at a sweep rate of 2 mV s^{-1}. It is noticed that the curves are symmetric closely to rectangular in shape, indicating an ideal capacitance behavior of reversible reaction. The SC of the as-prepared samples decreases monotonically with the increase in K ion content, from 159 F g^{-1} for M2 to 131 F g^{-1} for M12. Fig. 9 shows the dependence of the SC value of the electrodes on the scanning rate. A decrease in SC with increasing sweep rate is observed for all samples, implying the decrease in the utilization efficiency of the active materials at high sweep rate.

In recent studies, it has been clearly shown that the values of SC are greatly affected by the surface process of the amorphous MnO_2 samples [34]. If the SC value is caused by the double-layer charging (adsorption) of cations on the surface of active materials, the SC values should be increased proportionally with the increase of specific surface area. Re-examining the surface value of the sample given in Table 1 shows that there is a great decrease in the surface area from M2 to M12 samples, but the SC values decreases only slightly from 159 F g^{-1} for M2 sample to 131 F g^{-1} for M12 sample. From the above results, it is inferred that the charge storage of the MnO_2 samples is more likely related to TSM. The details of tunnel structure and the contents of cations play the key roles for the SC value. This is in accord with our earlier study [2].

Since all the samples in the present work are in poorly crystalline state with various K contents, the decreased low value of SC is not due to the amorphous nature of the samples. The dependence of specific capacitance of as-prepared samples on molar ration of K to Mn is shown in Fig. 10. It is observed that the SC values are greatly influenced by the molar ration of K to Mn, especially when the molar ration is less than 0.1. When the molar ration of K to Mn is larger than 0.4, there is only little change in the SC values.

In order to explore the changes of K ion due to the electrochemical process, after two CV cycles the samples were potentiosated at 0 V or 1 V for 24 h, respectively. Fig. 11 exhibits the XPS spectra for the as-prepared samples. It should be noticed that the F1s peak is due to the binder (PTFE) during the electrode fabrication process. And the appearance of Na 1s peak clearly indicated the Na

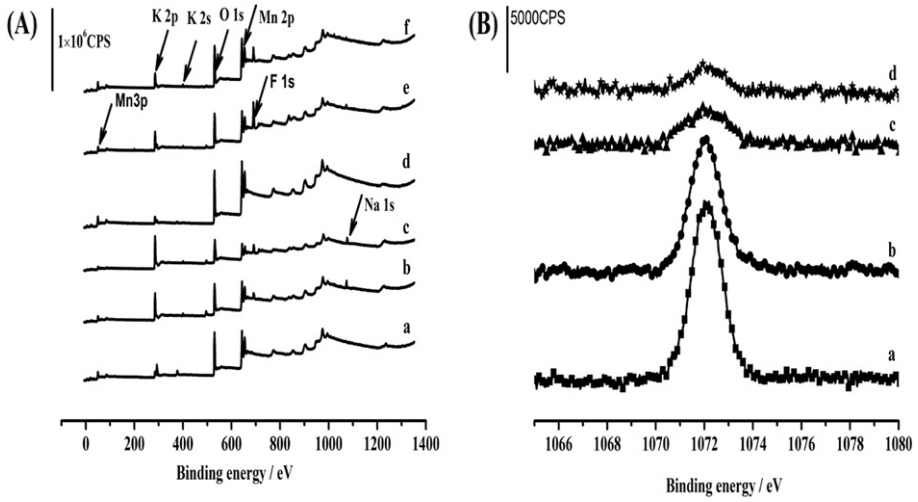

Fig. 11. (A) XPS spectra for samples of (a) M12, (b) M12-0V, (c) M12-1V, (d) M4, (e) M4-0V, and (f) M4-1V; (B) Enlarged Na 1s XPS spectra for samples of (a) M12-0V, (b) M12-1V, (c) M4-0V and (d) M4-1V.

Table 3
The Mn, O, and K content of the as-prepared samples.

At%	M12	M12-0V	M12-1V	M4	M4-0V	M4-1V
Mn	23.73	23.16	24.34	29.09	26.05	30.22
O	62.01	62.45	62.2	67.98	71.29	67.88
K	14.27	2.26	2.87	2.93	1.65	1.77
Na	0.00	12.13	11.59	0.00	1.01	1.13
K/Mn	0.60	0.10	0.12	0.10	0.06	0.06
Na/Mn	0.00	0.52	0.48	0.00	0.04	0.04

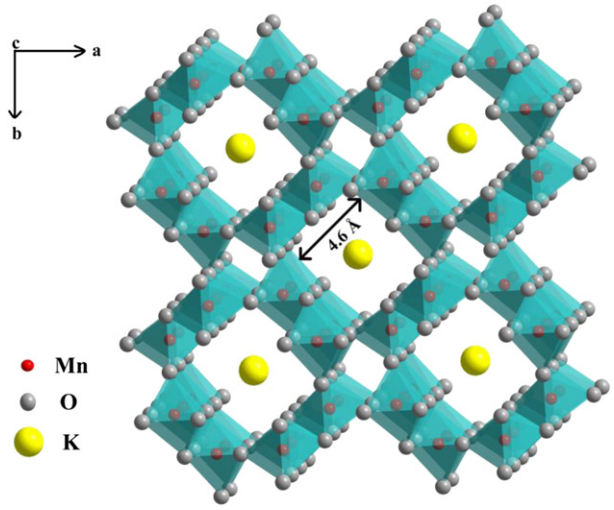

Fig. 12. Schematic diagram of the tunnel structure of α-MnO_2.

existence in all samples after potentiosated. Furthermore, the peak intensity of Na 1s of M12 is larger compared with that M4, both for 0 V and 1 V in Fig. 11(B). This implies that the level of Na ion content in M12 is higher than that in M4.

The K, Na, Mn and O contents of M4 and M12 after potentiosated at 0 V (M*x*-0V) and 1 V (M*x*-1V) for 24 h in 0.1 M Na_2SO_4 are presented in Table 3. The results of Mn and K were characterized by ICP elemental analyses and the content of O was tested by XPS analyses. From the results, it is clearly seen that the amount of K ions before potentiosated is equal to the sum of the amounts of K and Na ions after potentiosated, which shows that part of K ions in the channel is replaced by Na ions during electrochemical reaction.

The tunnel structure of α-MnO_2 is showed in Fig. 12. It is inferred firstly that when the K content is very low, it has no effect on the physical structure and available tunnel space. With more and more K was added into the tunnel, the physical structure and tunnel space change enormously, as shown in the SEM images of Fig. 2. The K ions occupied more and more tunnel space as shown by the values of the pore space given in Table 1 that causes the SC values to decrease as inferred from the TSM mechanism.

4. Conclusions

Unlike the traditional electric double-layer surface chemisorption mechanism, the SC of amorphous MnO_2 is predominant by the TSM mechanism. The intercalation and distribution of the K ions in MnO_2 play an important role in determining the SC values. The specific capacitance is decreased by 17.6%, from 157 F g^{-1} (M2) to 131 F g^{-1} (M12) with increasing K ion content. Furthermore, the more K ion in the tunnel, the less space available to alkaline metal cations (or protons) of the electrolyte to move into/from the tunnel of MnO_2, which caused the SC value to decrease with the increase in K ions. It is also found that part of K ions in the tunnels can be replaced by Na ions during electrochemical reaction.

Acknowledgments

We like to thank the financial support from National Nature Science Foundation of China under Grants (No. 51102139 and No. 50972065) and from Shenzhen Technical Plan Projects (No. JP200806230010A and No. SG200810150054A) are greatly appreciated. We also thank the financial support from Guangdong Province Innovation R&D Team Plan (2009010025) and from China Postdoctoral Science Foundation (No. 2012M510022).

References

[1] C. Xu, F. Kang, B. Li, H. Du, J. Mater. Res. 25 (2010) 1421–1432.
[2] D. Zhai, B. Li, C. Xu, H. Du, Y. He, C. Wei, F. Kang, J. Power Sources 196 (2011) 7860–7867.
[3] C.Z. Yuan, B. Gao, L.F. Shen, S.D. Yang, L. Hao, X.J. Lu, F. Zhang, L.J. Zhang, X.G. Zhang, Nanoscale 3 (2011) 529–545.
[4] J.T. Zhang, W. Chu, J.W. Jiang, X.S. Zhao, Nanotechnology 22 (2011) 125703.
[5] O. Ghodbane, J.L. Pascal, F. Favier, ACS Appl. Mater. Interfaces 1 (2009) 1130–1139.
[6] T. Brousse, M. Toupin, R. Dugas, L. Athouel, O. Crosnier, D. Belanger, J. Electrochem. Soc. 153 (2006) A2171–A2180.
[7] H. Huang, X. Wang, Nanoscale 3 (2011) 3185–3191.
[8] A.G. Pandolfo, A.F. Hollenkamp, J. Power Sources 157 (2006) 11–27.
[9] S.F. Wang, Z.C. Zhang, H.R. Liu, W. Zhang, Z. Qian, B.B. Wang, Colloid Polym. Sci. 288 (2010) 1031–1039.
[10] F.J. Liu, T.F. Hsu, C.H. Yang, J. Power Sources 191 (2009) 678–683.
[11] M. Jayalakshmi, K. Balasubramanian, Int. J. Electrochem. Sci. 3 (2008) 1196–1217.
[12] J. Desilvestro, O. Haas, J. Electrochem. Soc. 137 (1990) C5–C22.
[13] H.Y. Lee, J.B. Goodenough, J. Solid State Chem. 144 (1999) 220–223.
[14] S. Sarangapani, B.V. Tilak, C.P. Chen, J. Electrochem. Soc. 143 (1996) 3791–3799.
[15] S. Devaraj, N. Munichandraiah, J. Phys. Chem. C 112 (2008) 4406–4417.
[16] L.C. Zhang, Z.H. Liu, H. Lv, X.H. Tang, K. Ooi, J. Phys. Chem. C 111 (2007) 8418–8423.
[17] S. Chen, J.W. Zhu, X.D. Wu, Q.F. Han, X. Wang, ACS Nano 4 (2010) 2822–2830.
[18] Y.S. Ding, X.F. Shen, S. Gomez, H. Luo, M. Aindow, S.L. Suib, Adv. Funct. Mater. 16 (2006) 549–555.
[19] J.B. Fei, Y. Cui, X.H. Yan, W. Qi, Y. Yang, K.W. Wang, Q. He, J.B. Li, Adv. Mater. 20 (2008). 452–+.
[20] A.E. Fischer, K.A. Pettigrew, D.R. Rolison, R.M. Stroud, J.W. Long, Nano Lett. 7 (2007) 281–286.
[21] M. Wei, Y. Konishi, H. Zhou, H. Sugihara, H. Arakawa, Nanotechnology 16 (2005) 245–249.
[22] Q. Feng, K. Yanagisawa, N. Yamasaki, J. Porous Mater. 5 (1998) 153–161.
[23] M.M. Thackeray, Prog. Solid State Chem. 25 (1997) 1–71.
[24] S.L. Kuo, N.L. Wu, J. Electrochem. Soc. 153 (2006) A1317–A1324.
[25] S.C. Pang, M.A. Anderson, T.W. Chapman, J. Electrochem. Soc. 147 (2000) 444–450.
[26] X.H. Tang, H.J. Li, Z.H. Liu, Z.P. Yang, Z.L. Wang, J. Power Sources 196 (2011) 855–859.
[27] R. Liu, J. Duay, S.B. Lee, ACS Nano 4 (2010) 4299–4307.
[28] J. Yan, Z. Fan, T. Wei, J. Cheng, B. Shao, K. Wang, L. Song, M. Zhang, J. Power Sources 194 (2009) 1202–1207.
[29] X.-H. Yang, Y.-G. Wang, H.-M. Xiong, Y.-Y. Xia, Electrochim. Acta 53 (2007) 752–757.
[30] C.J. Xu, H.D. Du, B.H. Li, F.Y. Kang, Y.Q. Zeng, Electrochem. Solid State Lett. 12 (2009) A61–A65.
[31] A.B. Yuan, Q.L. Zhang, Electrochem. Commun. 8 (2006) 1173–1178.
[32] R.N. Reddy, R.G. Reddy, J. Power Sources 124 (2003) 330–337.
[33] S.L. Brock, N.G. Duan, Z.R. Tian, O. Giraldo, H. Zhou, S.L. Suib, Chem. Mater. 10 (1998) 2619–2628.
[34] P. Ragupathy, H.N. Vasan, N. Munichandraiah, J. Electrochem. Soc. 155 (2008) A34–A40.
[35] M. Toupin, T. Brousse, D. Belanger, Chem. Mater. 16 (2004) 3184–3190.